Silicon (2019) 11:2919–2931
https://doi.org/10.1007/s12633-019-0083-6

ORIGINAL PAPER

# Machining and Characterization of Channels and Textures on Quartz Glass Using μ-ECDM Process

J. Bindu Madhavi [1] · Somashekhar S. Hiremath [1]

Received: 4 July 2018 / Accepted: 14 January 2019 / Published online: 24 January 2019


**Abstract**
Applications of various glass materials like sodalime, borosilicate and pyrex are growing in the field of micro-electro mechanical systems. Quartz glass composes of pure silicon dioxide which is well- known for its hardness and processing of it would widen the scope of its application in product miniaturization. Micro-Electro Chemical Discharge Machining (μ-ECDM) is a non-conventional hybrid technique which combines the features of Electro Chemical Machining (ECM) and Electro Discharge Machining (EDM). In the present paper, channels are machined using μ-ECDM on 4 mm thick quartz glass with 370 μm diameter stainless steel (SS) tool. Experiments are designed at various levels of voltage (V), electrolyte concentration (wt%C) and duty factor (%DF) for parametric study. Signal to Noise (S/N) ratio and Grey Relational Analysis (GRA) are used to optimize the process parameters to enhance responses individually and simultaneously. The obtained S/N ratio optimized parameters to maximize Material Removal Rate (MRR) are - 60 V, 30 wt%C, 60 %DF resulted in 753 μg/min, to minimize Tool Wear Rate (TWR) are – 40 V, 20 wt%C, 50 %DF resulted in 2.99 μg/min and to minimize width of the channel are- 40 V, 20 wt%C, 60 %DF resulted in 500 μm. The GRA optimized parameters are- 40 V, 20 wt%C and 50 %DF resulting in 81 μg/m of MRR, 2.99 μg/m of TWR and 557.6 μm of width with entropy technique- equal weightage. Further an attempt has been made to machine texture on the quartz surface which is still in its early stages of research. GRA optimized parameters as detailed above are used to machine channels and generate textures of 45° hatch, square hatch and 45° criss-cross hatch on quartz glass.

**Keywords** Micro-electro chemical discharge machining · Quartz · Material removal rate · Tool wear rate · Width of channel · Signal to noise ratio · Grey relational analysis · Texture

## 1 Introduction

Due to the unique chemical, thermal and mechanical properties of glass materials, they are consistently used in the field of micro-fluidics as reservoirs, inlet and outlet ports in a vapor source of micro-gas chromatograph systems [1], as apertures for artificial lipid bilayer fluidic device [2], in micro-sensors and electronic devices as provision for electrical interconnection between the electrode pads, piezo-resistive element for sensing pressure [3] and modulated glass surface textures to trap light in solar cells [4]. Generating micro-features like holes, channels and textures on the glass in such applications are challenging by conventional and some non-conventional techniques. The μ-ECDM process is one among the non-conventional process has proved its potential application in machining glasses.

Figure 1 shows the ECDM processing cell - schematic diagram (Fig. 1a) and mechanism of material removal (Fig. 1b). It consists of a beaker, an electrolyte, an auxiliary electrode, a tool electrode and a workpiece. Electrolyte facilitates the electrical conductivity, formation of the gas film and aids in chemical etching. Researchers have studied different electrolytes and found that sodium fluoride (NaF), hydrochloric acid (HCl), sulfuric acid ($H_2SO_4$) results in negligible effect on material removal [5]. Sodium chloride (NaCl), sodium nitrate ($NaNO_3$) electrolytes results in sludge formations, contamination of electrolyte solution and lower MRR [6], whereas potassium hydroxide (KOH) and sodium hydroxide (NaOH) electrolytes results in smooth machined surfaces [5, 7]. The main properties of NaOH electrolyte like high specific conductance accelerated chemical reaction and gas bubble generation results in high material removal rate and calls for

✉ Somashekhar S. Hiremath
somashekhar@iitm.ac.in

[1] Department of Mechanical Engineering, Indian Institute of Technology Madras, Chennai, Tamil Nadu 600036, India

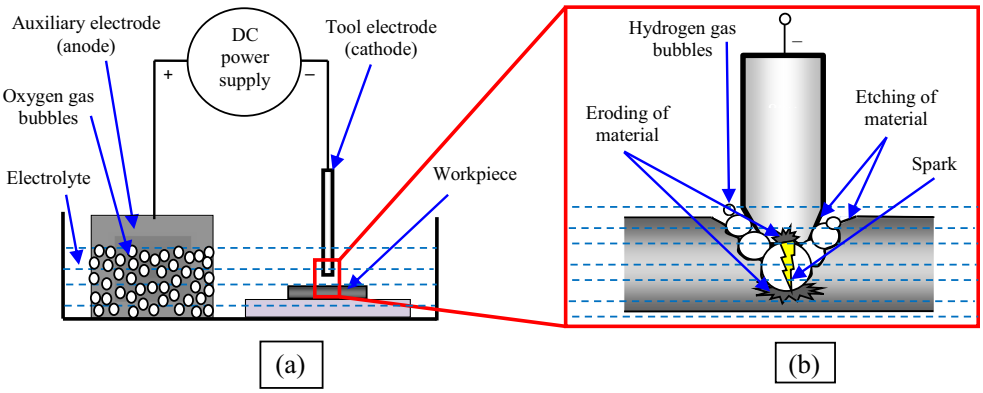


**Fig. 1** Schematic diagram of ECDM (**a**) processing cell (**b**) material removal mechanism

its wider application [8]. Similarly, most commonly used auxiliary electrode materials are of platinum in the form of foil [9], stainless steel and graphite in the form of the plate [10, 11]. Also note the size of auxiliary electrode should be hundred times larger in surface area than that of the tool electrode. This limits the dissolution process of anode material and ensures high spark density at tool tip [12]. Similarly the tool electrode used in ECDM process should possess certain characteristics like high conductivity, chemical inertness and stiffness to avoid erosion, etching, shape deterioration and bending. Stainless steel, tungsten carbide and brass are widely used tool materials in ECDM process. Out of which tungsten carbide results in lower TWR than that of stainless steel and brass. On the other hand, the stainless steel tool retain it shape without much deterioration and also an economical advantages as compared to brass and tungsten carbide [10]. Different types of tools - tubular, pointed tool tips and also the polarity of tools have been used to improve the machinability, accuracy and quality of the machined surface [13–15]. Similarly the effect of pulsed DC power supply and constant DC power supply have been studied and reported in the paper [16]. The prominent chemical reactions taking place during ECDM process are detailed [6] below:

- **Chemical reactions at anode - Evolution of oxygen gas bubbles and anodic dissolution**

The hydroxide ions from the alkaline electrolyte solution will form water and oxygen along with releasing electron as shown in Eq. (1):

$$4(OH)^{-} \rightarrow 2H_2O + O_2\uparrow + 4e^{-} \quad (1)$$

Auxiliary electrode is usually of chemically inert material (graphite in present work) and of larger surface area to avoid anodic dissolution.

- **Chemical reactions at cathode - Evolution of hydrogen gas bubbles and spark generation**

The electrons released from electrolyte acts on water molecules in the electrolyte solution to form hydroxide ions and hydrogen as shown in Eq. (2).

$$2H_2O + 2e^{-} \rightarrow 2OH^{-} + H_2\uparrow \quad (2)$$

This hydrogen gas bubbles coalescence to form a stable blanket of an ionized gas film which isolates the tool from the surrounding electrolyte. When the voltage is increased beyond a critical value, sufficient electrical resistance built up by the gas film breaks down. Then spark occurs due to the high current density at the tooltip and the surrounding electrolyte. The temperature generated by the spark discharge causes the workpiece material in its close vicinity: melt, vaporize and etched [17]. Also noted the shorter duration spark is more preferred as it increases the sparking frequency and current density which results in maximized MRR [7].

The following section elaborates the literatures concerned with μ-ECDM process used for generation of micro holes, micro channels and textures. Various researchers have studied the effect of machining parameters on various output responses. The machining parameters of interest are voltage, electrolyte concentration, duty factor etc. along with electrode and workpiece materials.

Wüthrich et al. [9] observed from the machined hole and channel on borosilicate glass that the machined hole diameter and width of the channel were found to be more than that of the tool diameter. Also depth of the channel was found to be more than given depth of cut. Details of the machining parameters and inferences are available in the literature.

Didar et al. [18] machined 15 mm length channels with 0.5 mm diameter SS tool, 110 mm SS ring anode, 30 wt% C NaOH on 1 mm thick soda lime glass. Standard deviation was calculated for 4–5 trials of each experiment. They found that with increase in machining time resulted in increased depth of the channel. Channel machined at 28 V and 5 μm/s for 15 min resulted in ~220 μm depth and as the machining time increased to 45 min resulted in ~280 μm depth of channel. They also found that as voltage was varied, depth of channel also increased. Channel machined at 28 V and 10 μm/s

resulted in ~80 μm depth and on increased voltage to 30 V resulted in ~120 μm depth. They varied feed rate and found that as feed rate increased, depth of channel decreased. Channel machined at 28 V and 10 μm/s resulted in ~80 μm depth and on increased feed rate to 40 μm/s resulted decreased depth to ~20 μm. They also observed that varying depth at different length of machined channel. Channel machined at 28 V and 10 μm/s resulted in 90 μm depth at 3 mm from the start of the machined channel and 110 μm depth at 12 mm distance. As the stand-off distance (SOD) was varied it was found that at 5 μm SOD the obtained depth of the channel at 3 mm from start of the channel was 53 μm and at 12 mm the depth was found to be ~ 48 μm. As the SOD increased to 10 μm resulted in 48 μm depth at 3 mm from start of the channel and 60 μm at the 12 mm distance.

Paul et al. [19] conducted $L_9$ experiments to machine channels on sodalime glass and modeled the process using Response Surface Methodology. Tungsten carbide tool of 300 μm diameter with NaOH solution as electrolyte and graphite plate as auxiliary electrode was used for machining. They found that MRR, TWR and heat affected zone (HAZ) increased with increase in voltage and concentration. Higher MRR, lower TWR and lower HAZ were obtained at 60 V, 25 wt% C and 60% DF. Higher concentration of 25 wt% resulted in stable gas bubble layer around the tool and higher voltage like 60 V increased the gas bubble generation rate which resulted in increased MRR of 2.8 mg/h. This also increased the temperature and side sparking at the tooltip which resulted in higher TWR of 0.3 mg/h and HAZ to 0.095 mm.

Jana et al. [20] machined channels of 3 mm length on soda lime glass with SS needle as tool of 500 μm diameter, SS ring as anode and NaOH as electrolyte. Channels machined at 30 V, 10 wt% C, 5 μm SOD with varying feed rate (FR) of 10 μm/s and 20 μm/s resulted in channel depth of 23 μm and 12 μm respectively. The obtained texture of machined surface of channel was of feathery pattern. Channels machined at 30 V, 5 μm SOD with varying concentration of 10 wt%, 20 wt%, 30 wt% and 40 wt% resulted in channel depths of 13 μm, 18 μm, 30 μm and 40 μm respectively. A texture of tori and redeposited melt glass was obtained due to tool movement. As the voltage was increased to 32 V resulted in 5 μm deeper channel than 30 V. Channel machined at 30 V, 10 wt% C, 5 μm/s with varying duty factor of 20%, 40%, 60%, and 80% resulted in increased glass temperature of 100 °C, 200 °C, 300 °C and 400 °C respectively. The channel surface thus obtained was from thick branched to thin branched texture.

The above literature survey reveals the potentials of μ-ECDM process while machining glasses like sodalime, borosilicate and pyrex materials. Quartz is now gaining its attention in research field and needs to be explored more through μ-ECDM process. Most of the literature has focused on the parametric study and its effects on enhancing process responses individually. As optimization of parameters to simultaneously enhance the responses is still a challenging task. Also it is noticed from the literature that texturing was investigated as a result of the layout formed (electrolyte flow and tool movement) inside a machined channel surface and not as machining features to generate textures on the surface of workpiece. Hence, it is observed that, machining of texture on non-conductive materials is at its early stage and need to be explored more. Considering this fact into account, the present research paper includes in-depth experimental investigation to machine channels and optimizes the process parameters to enhance the machining responses individually and simultaneously. Further various textures are machined using μ-ECDM setup on the quartz glass with an optimized parameters.

## 2 Experimental Setup and Experimentation

Figure 2 shows the schematic diagram of μ-ECDM experimental setup. It consists of DC power supply, processing cell and tool feeding unit with other monitoring instruments. A pulse generating circuit supplies a pulsed voltage between the tool and an auxiliary electrode. The inter-electrode gap is about 30 mm. The level of the electrolyte solution in the processing cell is maintained about 2 mm above the top surface of the immersed workpiece. A bipolar stepping motor actuated tool feeding mechanism provides the Z axis motion to the tool. The processing cell is mounted on the X-Y scanning stage. The X-Y and Z motions are controlled through micro-stepping motor driver - USB connected graphical user interface. Figure 3 shows the photographic view of the developed μ-ECDM experimental setup.

### 2.1 Pilot- Stage Experimentations

Pilot- stage experiments have been carried out with stainless steel wire tool of 370 μm diameter and quartz glass of 20 mm × 20 mm × 4 mm as the workpiece. The workpiece surface attains the replica shape of the tooltip, a flat shape tooltip was used for machining channel layer by layer in order to achieve a flat machined channel surface. The machining parameters of interest are type of electrolyte, electrolyte concentration, voltage and duty factor. Initial channels are machined with 60 V, 20 wt% C, 0.01 mm/s FR and 60% DF and two types of electrolytes- NaOH and KOH of 20 wt% C. The obtained channels are shown in Fig. 4. The channels machined with KOH electrolyte resulted in smaller width and clear edges as compared to NaOH as electrolyte. Hence further studies are carried out with KOH electrolyte. Next, channels are machined with 60% DF, 20 wt% C KOH and 0.01 mm/s FR with continuously varying voltage from 35 V-65 V. This experimentation reveals that channels machined

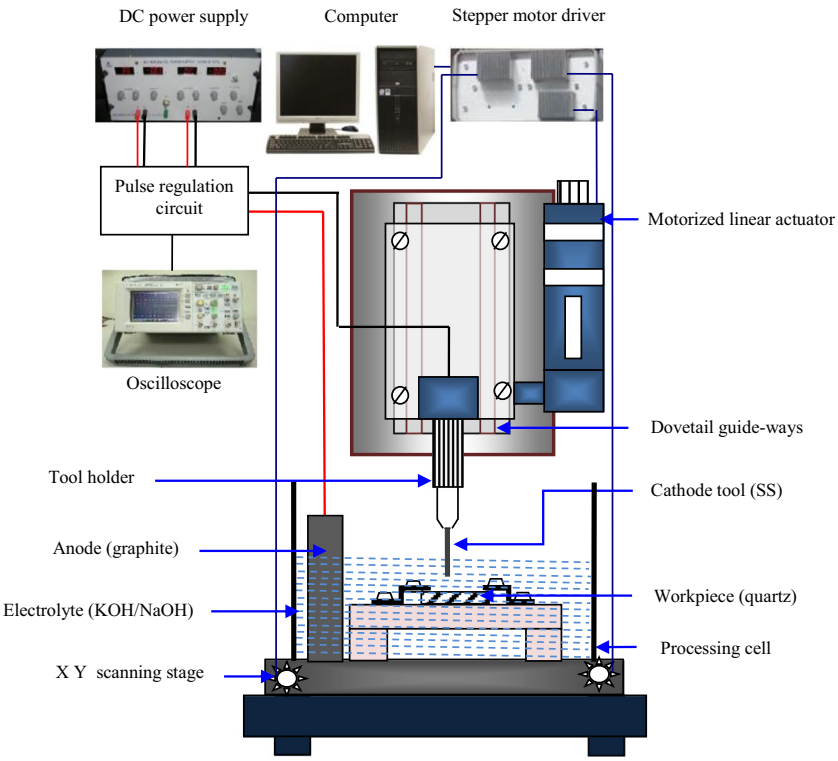


**Fig. 2** Schematic of the μ-ECDM experimental setup

below 40 V resulted in lower MRR, tool bending and scratching the surface while the channels machined above 60 V resulted in increased TWR. Hence, the voltage range has been fixed from 40 V to 60 V. Further channels are machined with 40 V, 20 wt% C KOH and 0.01 mm/s FR with varying duty factor. This experimentation reveals that channels machined below 35% DF resulted in straggled and discontinuous channels while the channels machined above 65% DF resulted in increased TWR and incomplete machined channels. Hence, the duty factor range has been fixed from 40% to 60%. Similarly channels are machined with 40 V, 0.01 mm/s FR and 40% DF with varying wt% concentration. This experimentation reveals that channels machined below 20 wt% C resulted in struggled and discontinuous channels while channels machined above 30 wt% C resulted in increased TWR and generated distorted and incomplete channels. Hence, the concentration range has been fixed from 20 wt% C to 30 wt% C.

## 2.2 Experimental Layout Plan

Table 1 shows the important physical and process parameters considered for the present study. Parametric combinations are designed based on $L_9$ Taguchi Orthogonal Array (OA). The process responses of interest are MRR in μg/min, TWR in μg/min, Aspect Ratio (AR)- depth to width of a machined

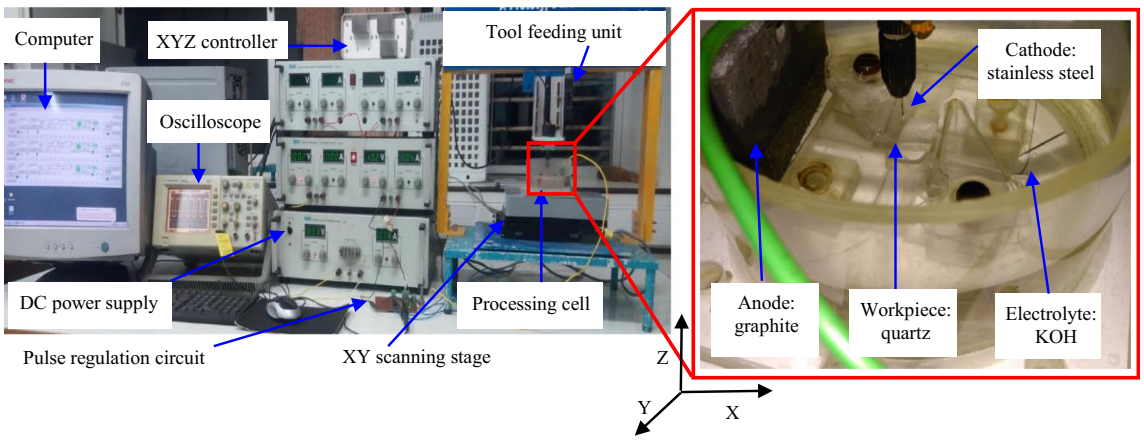


**Fig. 3** Photographic view of the μ-ECDM experimental setup

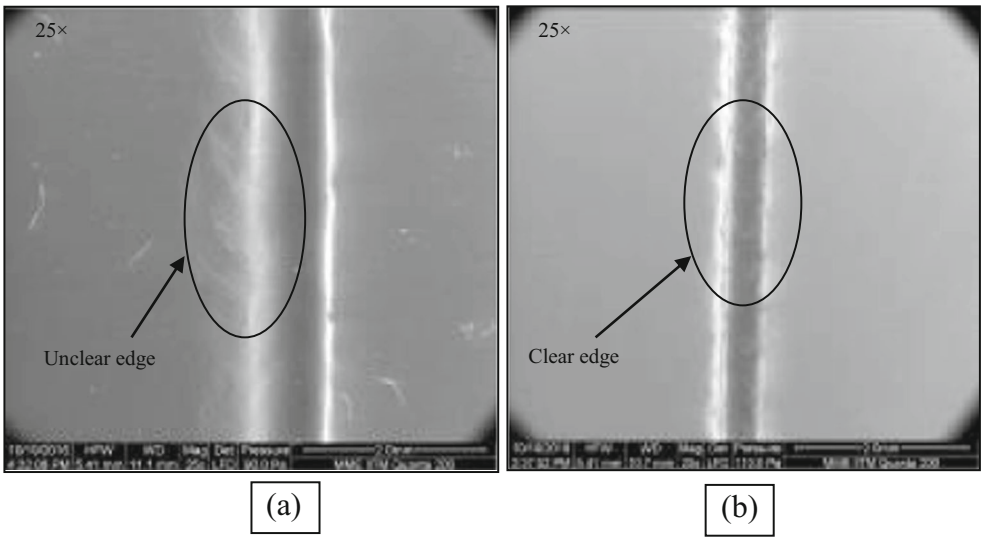


**Fig. 4** Channels machined with 60 V, 20 wt% C, 60% DF and 0.01 mm/s FR (a) NaOH electrolyte (b) KOH electrolyte

channel and surface roughness (Ra) in microns. Here, MRR and TWR are the measures of difference in weight of workpiece and tool before and after machining with respect to machining time. Mettler Toledo Electronic weighing balance is used for accurate measurement of MRR, TWR and NaOH pallets. The generated quality of the machined inside channel surface and edges are characterized using confocal microscope – OLYPUS LEXT LS 4000. The depth and surface roughness are measured using non-contact optical surface profiler - BRUKER Contour GT InMotion, while the width of the machined channels are measured using Scanning Electron Microscope (SEM) - QUANTA 200.

The channels are machined layer by layer of approximately 10 mm length with 0.1 mm depth of cut (DOC) per pass. Total number of passes maintained to be 2 for each set of experiment. Each channel is divided into three parts for characterization. Two parts from the ends of the channel of 2 mm each are ignored in order to avoid boundary effects and the middle part of the channel of 6 mm is considered for characterization.

Signal to Noise ratio optimization technique has been used for process parameters with an objective of improving the individual responses like higher MRR -'higher the better', Lower TWR and lower width of the channel- 'lower the better' using the following equations and same equations were used in the literature [21].

Higher the better−MRR

$$S/N = -10 \times \log_{10}\left(\frac{1}{n}\right)\sum_{i=1}^{n}\frac{1}{(MRR_i)^2} \tag{3}$$

Lower the better−TWR or ROC

$$S/N = -10 \times \log_{10}\left(\frac{1}{n}\right)\sum_{i=1}^{n}\left((TWRorROC)_i\right)^2 \tag{4}$$

where, $n$ is the number of trials for each experiment and $i$ is the present value.

Similarly, the grey relational analysis optimization technique has been used with an objective of improving multiple responses like higher MRR with lower TWR and lower width of the machined channels. Table 2 shows the procedural steps and equations involved in GRA. Responses can be prioritized by allocating weightages depending on the requirement of the situation or considering it equal to one or by entropy technique - equal weightages to the output responses [22]. In present work, entropy technique has been used to strike out the balance between the output responses.

**Table 1** Physical and process parameters to machine channels on quartz workpiece

| | | | |
|---|---|---|---|
| Physical parameters | | | |
| Processing cell | Acrylic beaker- 100 mm diameter and 50 mm height | | |
| Workpiece | Quartz glass (20 × 20 × 4) mm | | |
| Cathode tool electrode | Stainless steel- 370 μm diameter, Feed rate- 0.01 mm/s | | |
| Anode auxiliary electrode | Graphite plate (50 × 40 × 5) mm | | |
| Electrolyte | Aqueous solution of KOH | | |
| Design of experiments (DOE) | Taguchi $L_9$ | | |
| Optimization technique | Signal to Noise Ratio, Grey Relational Analysis | | |
| Process Parameters | | | |
| Levels | 1 | 2 | 3 |
| Voltage (V) | 40 | 50 | 60 |
| Duty Factor (%) | 40 | 50 | 60 |
| Concentration (wt%) | 20 | 25 | 30 |

**Table 2** Procedural steps and equations involved in GRA

| Sl. No. | Procedure | | Equations |
|---|---|---|---|
| 1 | Normalization: Response value is converted to a comparable range between 0 and 1 | Larger the better | $\eta_i = \frac{MRR_i - MRR_{\min}}{MRR_{\max} - MRR_{\min}}$ |
| | | Smaller the better | $\eta_i = \frac{TWR_{\max} - TWR_i}{TWR_{\max} - TWR_{\min}}$ |
| | | Smaller the better | $\eta_i = \frac{Width_{\max} - Width_i}{Width_{\max} - Width_{\min}}$ |
| 2 | Deviation Sequence: To obtained deviation of each normalized value from its desired value (i.e. 1) | | $\delta_i = \mid \eta_{\max} - \eta_i \mid$ |
| 3 | Grey Relation Coeficient (GRC): To obtained relationship between the desired and actual normalized experimental results | | $\gamma_i = \frac{\delta_{\min} + \xi\delta_{\max}}{\delta_i + \xi\delta_{\max}}$ distinguishing coefficient, $\xi = 0$ to 1; considered to be 0.5 |
| 4 | Weightage: To prioritize responses by entropy technique [22] | | $w_j = \frac{\frac{1}{m-S}[1-s]}{\sum \frac{1}{m-S}[1-s]}$ number of responses, $m = 3$ summation of entropy, $S = \sum_{i=1}^{n} s_i$ entropy function of each response, $s_i = \upsilon \sum_{i=1}^{n} f(\psi_i)$ mapping function of 's', $f(\psi_i) = \psi_i e^{(1-\psi_i)} + (1-\psi_i)e^{\psi_i} - 1$ variable, $\psi_i = \frac{GRC_i}{\sum_{i=1}^{n} GRC_i}$ normalized coefficient, $\upsilon = \frac{1}{(e^{0.5}-1)n}$ |
| 5 | Grey Relation Grade (GRG): Transfer GRC of all the responses to a weightaged single comparable sequence | | $\lambda_i = \frac{1}{N} \sum_{i=1}^{N} (w_i \gamma_i)$ |
| 6 | Average GRG: To obtain preferred (highest) level for each parameters | | $\overline{\lambda}_i = \frac{1}{N} \sum \lambda_{i(MRR/TWR/Width)}$ |
| 7 | Optimized parameters | | $\overline{\lambda}_{P_{\max}}$ |
| 8 | Order of parametric significances | | $\left(\overline{\lambda}_{P_{\max}} - \overline{\lambda}_{P_{\min}}\right)_{\max}$ |

## 3 Results and Discussions

### 3.1 Machining of Channels with Varying Process Parameters

Table 3 shows the experimental layout of the process parameters and the obtained response values. It is observed from the Table that 1st experimental combination*:* 40 V, 20 wt% C and 40% DF resulted in lower TWR of 2.99 μg/min, lower width of 460.3 μm and also lower MRR of 77.684 μg/min which is not a desirable aspect as productivity improvement is concerned. This can be due to lower intensity of discharge available for shorter duration resulting in lower temperature at the tool tip for eroding the tool and workpiece material. Also the lower electrolyte concentration and hence the specific conductivity of electrolyte reduces the etching of these materials.

The 9th experimental combination: 60 V, 30 wt% C and 50% DF resulted in higher MRR of 299.94 μg/min, higher TWR of 51 μg/min and higher width of 1000 μm which is also not desirable aspects. This may be due to increase in intensity of discharge, side spark, higher electrolyte concentration and hence the specific conductivity of electrolyte increases the etching of these materials.

Figure 5 shows all the nine machined channel images of SEM, optical surface profiler and confocal microscope with Ra, width, depth and AR values. It was

**Table 3** Experimental layout of the process parameters and obtained response vaules

| Ex. No | Parameters | | | Responses | | |
|---|---|---|---|---|---|---|
| | V | wt% C | % DF | MRR (μg/min) | TWR (μg/min) | Width (μm) |
| 1 | 40 | 20 | 40 | 077.684 | 2.990 | 460.3 |
| 2 | 40 | 25 | 50 | 094.781 | 3.299 | 500.3 |
| 3 | 40 | 30 | 60 | 132.573 | 4.499 | 504.0 |
| 4 | 50 | 20 | 50 | 92.381 | 5.990 | 503.0 |
| 5 | 50 | 25 | 60 | 139.772 | 10.198 | 587.0 |
| 6 | 50 | 30 | 40 | 140.072 | 19.000 | 676.9 |
| 7 | 60 | 20 | 60 | 203.059 | 26.390 | 647.8 |
| 8 | 60 | 25 | 40 | 209.958 | 49.129 | 892.0 |
| 9 | 60 | 30 | 50 | 299.940 | 51.000 | 1000.0 |

V: Voltage; C: Electrolyte Concentration (wt%); DF: Duty Factor (%); MRR: Material Removal Rate; TWR: Tool Wear Rate

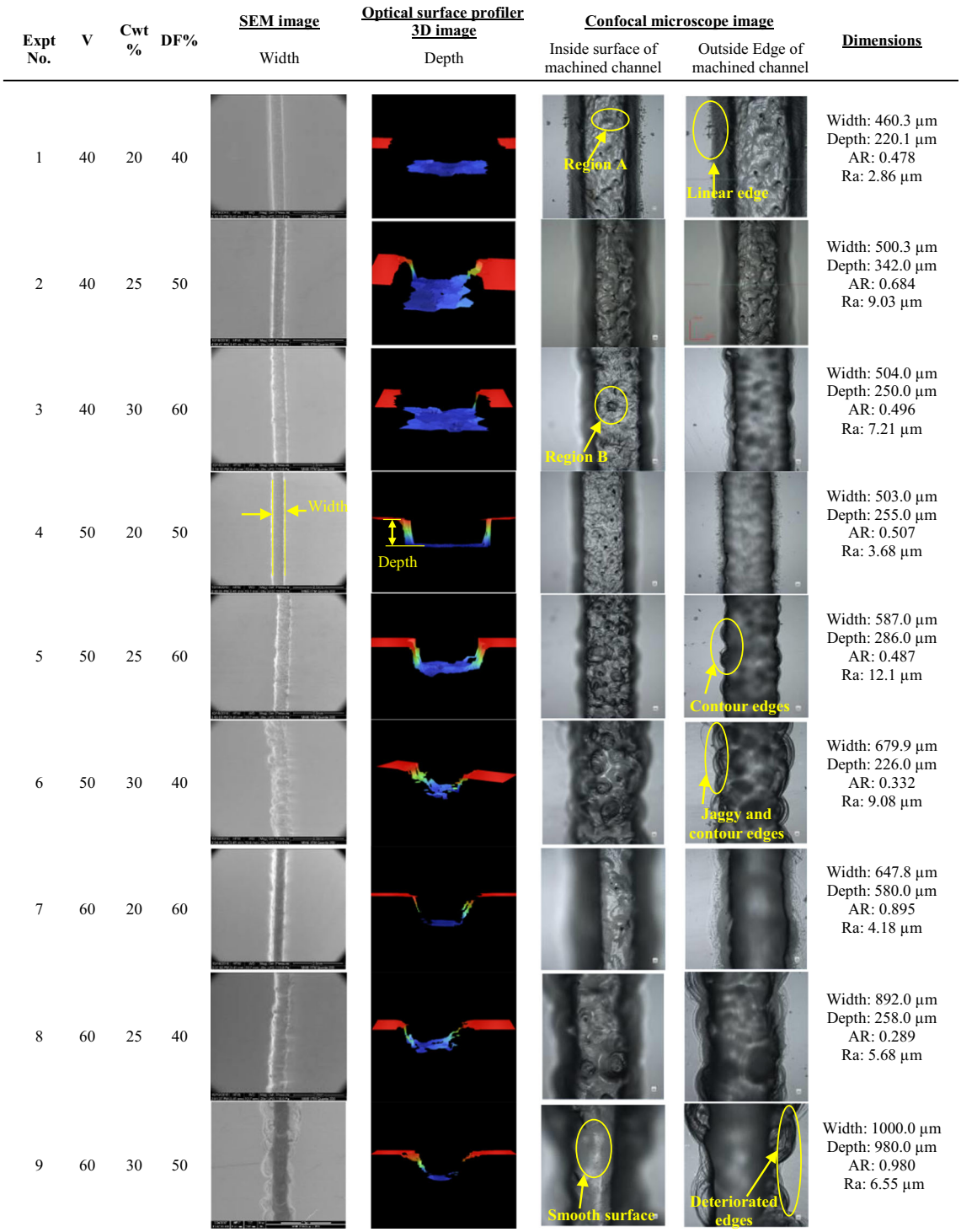


**Fig. 5** Images of the machined $L_9$ channels with width, depth, AR and Ra values: SEM (25×), Profiler (10.87×) and Confocal (10×)

found that lower machining parameters: 40 V, 20 wt% C and 40% DF of 1st experiment resulted in lower Ra of 2.86 µm, lower width of 460.3 µm, lower depth of 220.1 µm which is closer to the given DOC 200 µm and smooth linear edge channel. As the level of parameters increased to 60 V, 30 wt% C and 50% DF of 9th experiment, it was observed that, Ra increased to 6.55 µm, width increased to 1000 µm, depth increased to 980 µm and also AR increased to 0.980 with distorted channel edges which are not desirable aspects. This can be due to stray erosion which occurs at the surface just adjacent to the machining area.

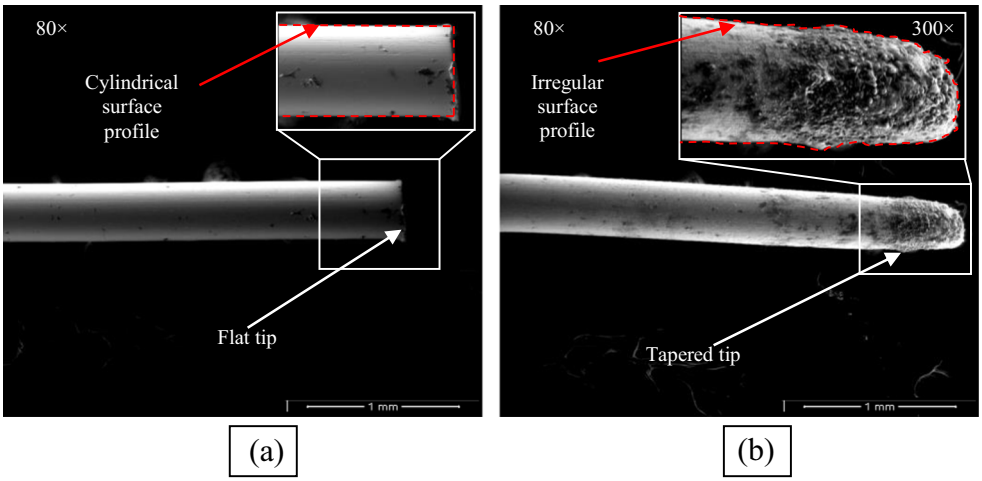


**Fig. 6** SEM image of the tool tip (**a**) before machining (**b**) after machining with experimental conditions- 60 V, 30 wt% C, 50% DF

Considering the concentration of electrolyte as constant parameter (20 wt%) with increasing voltage and duty factor (ref. experiment no 1, 4 and 7) it can be observed that the Ra, width, depth and AR are continuously increasing and linear channels edges tends to become slightly contoured. This can be due to high intensity of discharge for longer duration.

Considering duty factor as constant parameter (40%) with increasing voltage and concentration (ref. experiment no 1, 6 and 8) it can be observed that the width, depth and AR continuously increases and the linear channels edges tends to become jaggy and contoured. This can be due to increase in material removal as a cause of increase in intensity of spark and specific conduction of electrolyte. Also experiment 6, resulted in higher Ra as compared to experiment 1 and 8 and this can be due to higher voltage (60 V) and concentration (30 wt% C) causing higher pronounced eroding and erosion. This also increases viscosity during machining and creates homogenization effect [19].

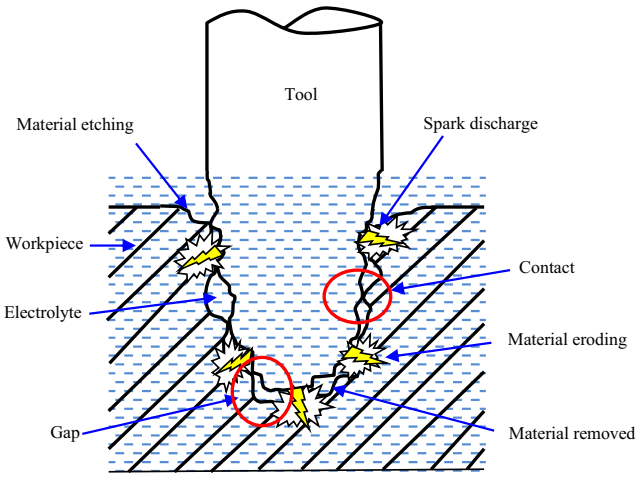


**Fig. 7** Schematic diagram of tool and workpiece interaction during machining

Considering voltage as constant parameter (40 V) with increasing concentration and duty factor (experiment no 1, 2 and 3) it can be observed that width continuously increases. This can be due to increase in specific conduction which increases etching rate and erosion rate for longer duration. As compared to experiment 1 and 3, experiment 2 resulted in higher Ra, depth and AR values. This can be due to the combined effect of lower intensity of spark at 40 V for moderate period 50% DF and specific conductivity 25 wt% C.

On observing the 3D images of the channels of experiments from 1 to 3, 4 to 6 and 7 to 9, it was found that, the side walls of the machined channels tapered and the machined surface of the channels became irregular. This may be due to the fact that as the machining progressed for higher depths, the tool worn out and deteriorated to form a tapered tip losing its flat tip as shown in Fig. 6. This causes the channel walls to attain approximately a replica shape of the tapered tool throughout its depth of machining. But, irregular surface profile of the tool and the channel (side walls and surface of the channel) are not a perfect replica of each other and thus creates gaps and contacts at random locations with each other. Referring to Fig. 7, the gap at some places favors material removal and the contact at other places no material removal occurs [23]. Thus, formation of tapered tool surface is an inherent property of the machining process.

Throughout the experiments feed rate of 0.01 mm/s is maintained kept constant. As a result, the machined channels surfaces are all almost similar as seen from the confocal images of Fig. 5 and also the same type observation was made in the literature [13]. During pulse on time, the high temperature sparks melts the workpiece material and piles up around the tool tip. During pulse off time, this piled up material cools and resolidifies around the tool tip as shown in region A. As the machining progresses, tool bends to overcome region A and stumbles to a new position; penetrating into the workpiece surface causing a pit formation as shown in region B. It is also observed that,

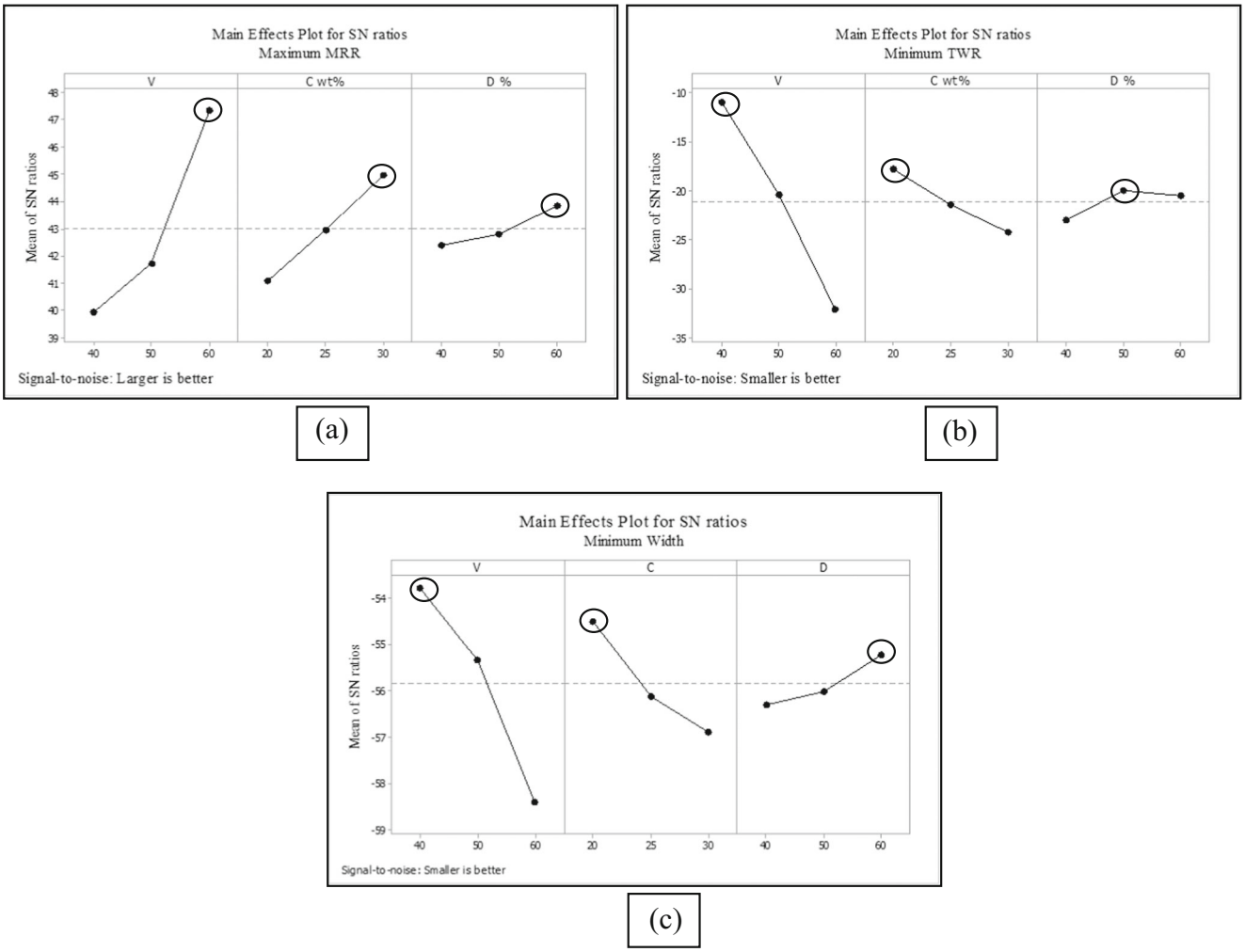


**Fig. 8** Main effects plot for S/N ratios of responses: (**a**) MRR (**b**) TWR (**c**) Width

region A and region B continues to occur forming an irregular pattern on the machined surface of the channel. This can be due to combined effect of the following reasons:

- Stumbling of tool at region A to a new position to form region B.
- Spark generated from random locations of the flat circular surfaced tool tip which strikes the surface of the workpiece [24].
- Continuous advancement of machining results in striking of such randomly generated sparks to a new location on the workpiece.

**Table 4** Relative significance of the parameters on each response

| Response | Parameter | Max value of mean of S/N ratio | Min value of mean of S/N ratio | Delta (Max - Min) value of mean of S/N ratio | Order of significance |
|---|---|---|---|---|---|
| MRR | V | 47.38 | 39.93 | 7.45 | 1 |
| | C | 44.97 | 41.09 | 3.88 | 2 |
| | DF | 43.84 | 42.39 | 1.44 | 3 |
| TWR | V | −10.98 | −32.14 | 21.15 | 1 |
| | C | −17.83 | −24.26 | 6.43 | 2 |
| | DF | −20.02 | −22.97 | 2.95 | 3 |
| Width | V | −53.76 | −58.41 | 4.65 | 1 |
| | C | −54.51 | −56.89 | 2.38 | 2 |
| | DF | −55.22 | −56.29 | 1.08 | 3 |

MRR: Material Removal Rate; TWR: Tool Wear Rate; V: Voltage; C: Electrolyte Concentration (wt%); DF: Duty Factor (%)

**Table 5** GRA procedural steps values of the machined $L_9$ channels

| Normalization | | | Deviation sequence | | | GRC | | | GRG |
|---|---|---|---|---|---|---|---|---|---|
| MRR | TWR | Width | MRR | TWR | Width | MRR | TWR | Width | |
| 0.00 | 1.00 | 1.00 | 1.00 | 0.00 | 0.00 | 0.33 | 1.00 | 1.00 | 0.78 |
| 0.08 | 0.99 | 0.92 | 0.92 | 0.01 | 0.08 | 0.35 | 0.99 | 0.86 | 0.73 |
| 0.25 | 0.97 | 0.92 | 0.75 | 0.03 | 0.08 | 0.40 | 0.94 | 0.86 | 0.74 |
| 0.07 | 0.94 | 0.83 | 0.93 | 0.06 | 0.17 | 0.35 | 0.89 | 0.74 | 0.66 |
| 0.28 | 0.85 | 0.77 | 0.72 | 0.15 | 0.24 | 0.41 | 0.77 | 0.68 | 0.62 |
| 0.28 | 0.67 | 0.60 | 0.72 | 0.33 | 0.40 | 0.41 | 0.60 | 0.56 | 0.52 |
| 0.56 | 0.51 | 0.65 | 0.44 | 0.49 | 0.35 | 0.53 | 0.51 | 0.59 | 0.54 |
| 0.60 | 0.04 | 0.20 | 0.41 | 0.96 | 0.80 | 0.55 | 0.34 | 0.39 | 0.43 |
| 1.00 | 0.00 | 0.00 | 0.00 | 1.00 | 1.00 | 1.00 | 0.33 | 0.33 | 0.56 |

MRR: Material Removal Rate; TWR: Tool Wear Rate; GRC: Grey Relational Coefficient; GRG: Grey Relational Grade

Considering increase in voltage and electrolyte concentration from 40 V to 60 V and 20 wt% C to 30 wt% C, at each level it is observed that region B predominates the region A for the whole length of channel been machined.

### 3.2 S/N Ratio Technique for Individual Enhancement in Responses

Figures 8a-c show the optimized parametric combinations from Main Effects Plot for S/N ratio to enhance responses individually. As shown in Fig. 8a, maximum MRR can be achieved by optimized parametric combination of 60 V, 30 wt% C and 60% DF. Confirmation test was carried out to verify the adequacy of the obtained optimized parameters and was found to be 753 μg/min. This increase in MRR can be due to the combined effect of higher intensity of spark and specific conduction available to erode and etch the material for a longer duration.

As shown in Fig. 8b, minimum TWR can be achieved from optimized parametric combination of 40 V, 20 wt% C and 50% DF. Confirmation test resulted in TWR of 2.994 μg/min which was found to be approximately same as that of 1st experiment. This can be due to the effect of lower intensity of spark available for a moderate duration at the tool tip. In addition, lower specific conduction of the electrolyte solution causes less erosion of tool material.

As shown in Fig. 8c, minimum width can be achieved from optimized parametric combination of 40 V, 20 wt% C and 60% DF. Confirmation test resulted in width of the channel to be 460 μm. This can be due to combined effect of lower intensity of spark for a longer duration with lower specific conduction of the electrolyte, reduces the side sparking and aids to achieve reduced width of channel.

Table 4 shows the relative significance of the parameters on each response. From the order of delta values, voltage (1st order) was found to be the most significant parameter affecting the responses, followed by concentration (2nd order) and then duty factor (3rd order).

**Table 6** Average of GRG and its order of parametric significance

| Parameter | Level 1 | Level 2 | Level 3 | Max-Min | Order of Significance |
|---|---|---|---|---|---|
| V | 0.749 | 0.600 | 0.509 | 0.240 | 1 |
| C | 0.660 | 0.593 | 0.578 | 0.083 | 2 |
| DF | 0.575 | 0.650 | 0.633 | 0.074 | 3 |

V: Voltage; C: Electrolyte Concentration (wt%); DF: Duty Factor (%)

### 3.3 GRA Technique for Simultaneous Enhancement in Responses

Table 5 shows the GRA procedural steps values of the machined $L_9$ channels showing GRC and GRG values calculated using the equations quoted in Table 2. Table 6 shows the average of GRG and its order of parametric significance. The obtained highest average GRG value corresponding to its parametric levels were: 40 V, 20 wt% C, 50% DF for simultaneously enhancing all the responses. As this parametric combination is same as that of S/N ratio for minimum TWR, the obtained responses were MRR of 81 μg/min, TWR of 2.99 μg/min and width of 557.6 μm. The parametric significance from GRA technique was found to be in the same order as that of S/N ratio technique i.e. voltage followed by concentration and then duty factor.

## 4 Machining of Texture on Quartz Glass

### 4.1 Pattern Layout and Dimensional Description

Figure 9 shows the texture layout and design description of the suggested textures on quartz surface: 45° hatch, square hatch and 45° criss-cross hatch. The variables describing the hatched patterns are- t: tool diameter; d: lateral increment of the machining (unmachined surface); θ: machining angle; L: total length of the machined texture and W: total width of the machined texture.

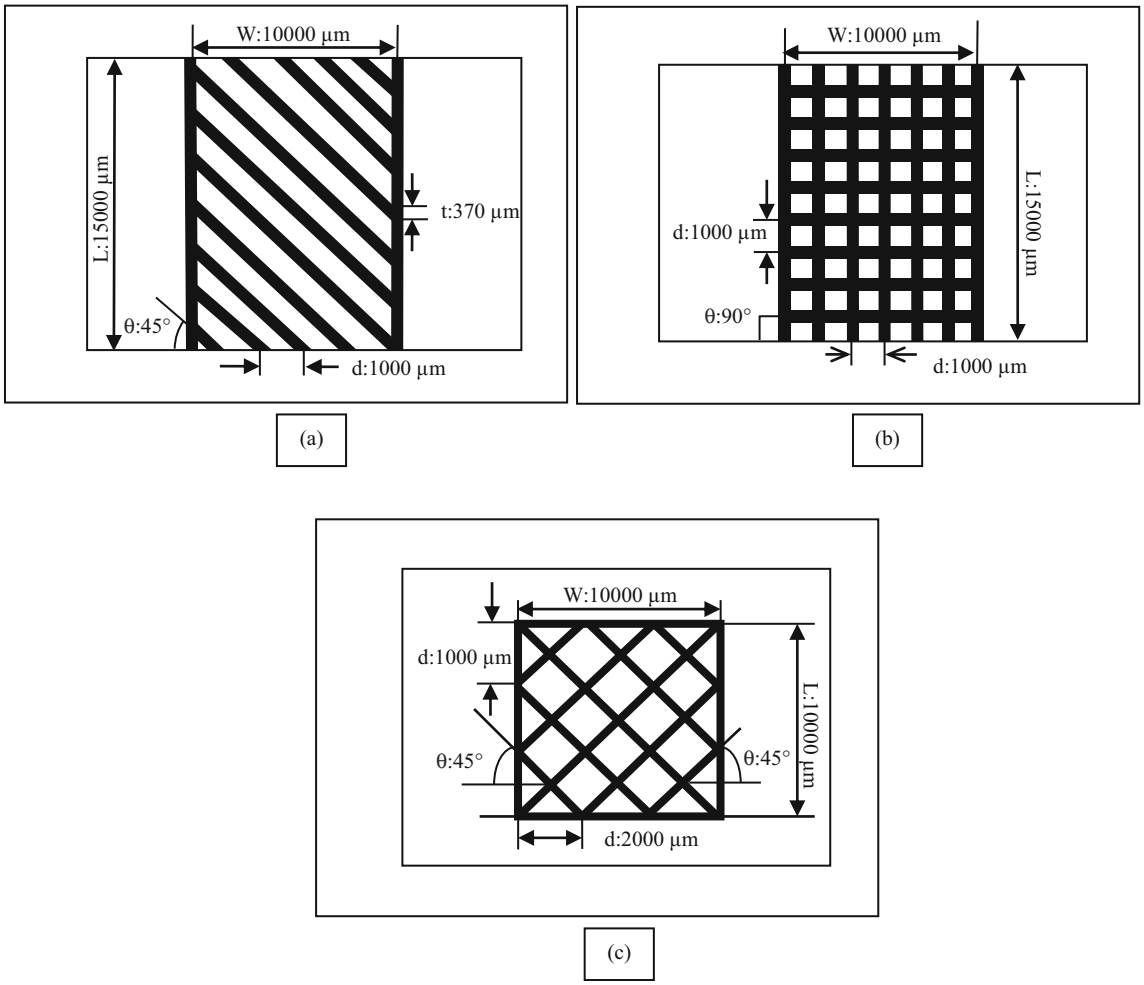


**Fig. 9** Texture layout and design description of the suggested textures on quartz surface: (**a**) 45° hatch (**b**) square hatch (**c**) 45° criss-cross hatch

### 4.2 Machining of Textures on Quartz Glass

Machining of textures have been carried out with GRG optimized parameters: 40 V, 20 wt% C and 50% DF.

### 4.3 Topographical Analysis

Figure 10 shows the SEM images of the machined micro-textures on quartz glass: 45° hatch, square hatch and 45° criss-cross hatch. The machined surface generated at region 1 is similar to the region B as depicted from the confocal image of Fig. 5. The imprint obtained at region 2, 3 and 4, becomes wavy and filleted. During machining, the hot electrolyte near the vicinity of the tool within the channel walls over flows in outwards direction and results in etching of the machined channel edges to attain the uniform wavy imprints along the direction of the feed. Also it has been noted for SEM images that as the machining progresses, the tool wear out continuously and affects the shape of the textured pattern.

## 5 Conclusions

μ-ECDM is a non-conventional micro-machining technology based on thermal and chemical machining mechanism effectively used to machine several electrical non-conductive materials like various types of glasses, various types of ceramic materials etc. The experimentation carried out so far on developed μ-ECDM setup reveals that the material removal rate largely depends on type of workpiece and tool material, type of electrolyte, its concentration and temperature, applied volage and duty factor. The following are the main conclusions derived while maching channels with varying process parameters and textures generated on quartz glass:

1. Optimized parameter from S/N ratio technique to individually enhance responses are:

- Maximized MRR: 60 V, 30 wt% C, 60% DF and it resulted in 753 μg/min.
- Minimized TWR: 40 V, 20 wt% C, 50% DF and it resulted in 2.999 μg/min.

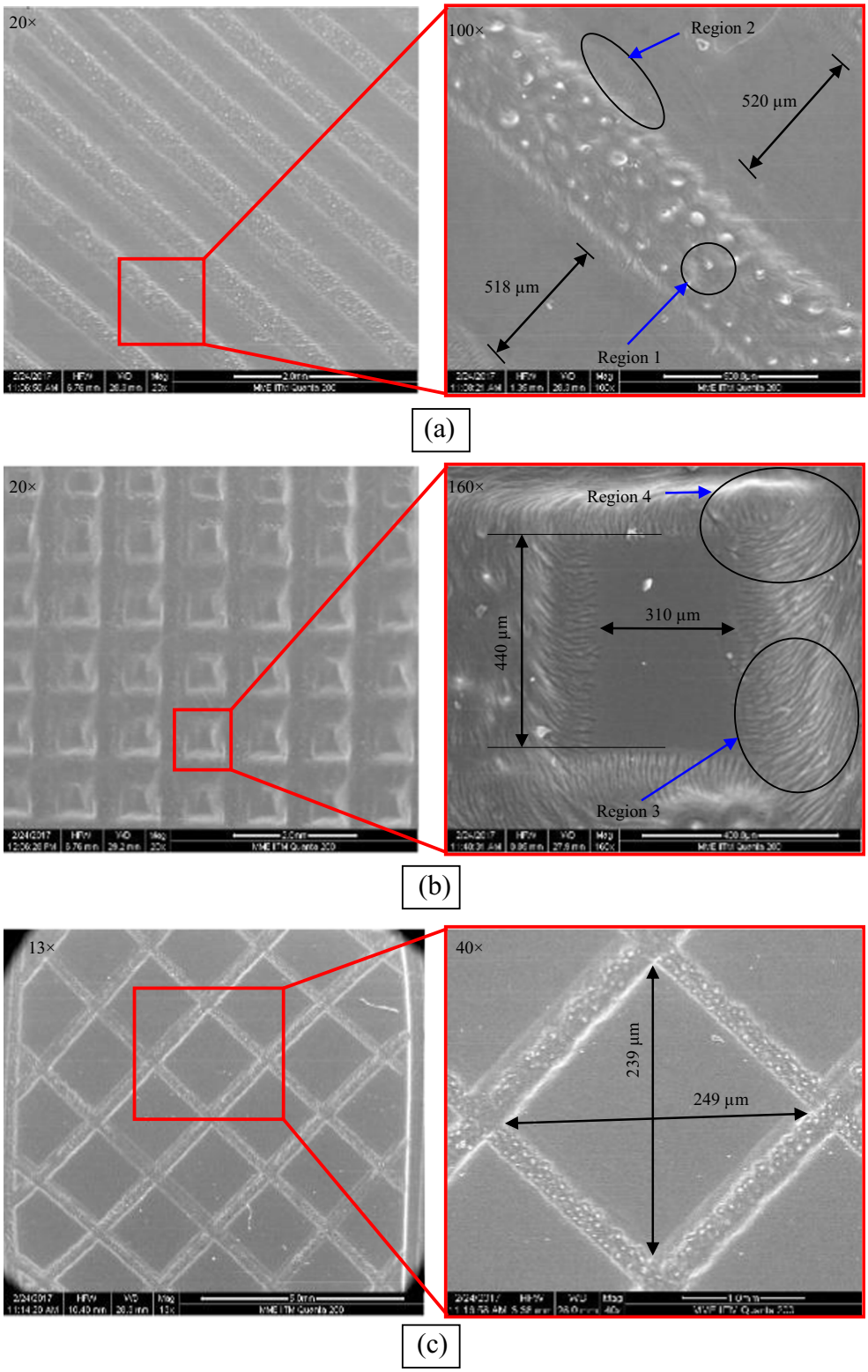


**Fig. 10** SEM topography images of surface micro textured on quartz: (**a**) 45° hatch (**b**) square hatch (**c**) 45° criss-cross hatch

- Minimized width of the channel: 40 V, 20 wt% C, 60% DF and resulted in 500 µm.

2. Optimized parameters from GRA to simultaneously maximize MRR, minimize TWR and minimize width of the channel (by entropy method- equal weightage): 40 V, 20 wt% C and 50% DF resulted in 81 µg/min of MRR, 2.99 µg/min of TWR and 557.6 µm of channel width.
3. GRA optimized parameters are successfully used to machine channels and generate textures on quartz glass: 45°

hatched micro-texture, 45° criss-cross hatched micro-texture and square hatched micro-texture. The detailed analysis are presented in the paper.



## References


1. Wallner JZ, Kunt KS, Obanionwu H, Oborny MC, Bergstrom PL, Zellers ET (2007) An integrated vapor source with a porous silicon wick. Phys Status Solidi 204:1449–1453. https://doi.org/10.1002/pssa.200674383
2. Sandison ME, Zagnoni M, Abu-hantash M, Morgan H (2007) Micromachined glass apertures for artificial lipid bilayer formation in a microfluidic system. J Micromech Microeng 17:S189–S196. https://doi.org/10.1088/0960-1317/17/7/S17
3. San H, Zhang H, Zhang Q, Yu Y, Chen X (2013) Silicon – glass-based single piezoresistive pressure sensors for harsh environment. J Micromech Microeng 23:075020. https://doi.org/10.1088/0960-1317/23/7/075020
4. Isabella O, Moll F, Krč J, Zeman M (2010) Modulated surface textures using zinc-oxide films for solar cells applications. Phys Status Solidi Appl Mater Sci 207:642–646. https://doi.org/10.1002/pssa.200982828
5. Cook NH, Foote GB, Jordan P, Kalyani BN (1973) Experimental studies in electro-machining. J Eng Ind 95:945–950. https://doi.org/10.1115/1.3438273
6. Bhattacharyya B, Doloi BN, Sorkhel SK (1999) Experimental investigations into electrochemical discharge machining (ECDM) of non-conductive ceramic materials. J Mater Process Tech 95:145–154. https://doi.org/10.1016/S0924-0136(99)00318-0
7. Crichton IM, McGeough JA (1985) Studies of the discharge mechanisms in electrochemical arc machining. J Appl Electrochem 15:113–119. https://doi.org/10.1007/BF00617748
8. Basak I, Ghosh A (1997) Mechanism of material removal in electroche machining: a theoretical model and experiment. J Mater Process Tech 71:350–359. https://doi.org/10.1016/S0924-0136(97)00097-6
9. Wuthrich R, Fascio V, Viquerat D, Langen H (1999) In situ measurement and micromachining of glass. Int Symp MICROMECHATRONICS Hum Sci IEEE:185–191. https://doi.org/10.1109/MHS.1999.820004
10. Behroozfar A, Razfar MR (2016) Experimental study of the tool Wear during the electrochemical discharge machining experimental study of the tool wear during the electrochemical discharge machining. Mater Manuf Process 31:574–580. https://doi.org/10.1080/10426914.2015.1004685
11. Ranganayakulu J, Hiremath SS, Paul L (2011) Parametric analysis and a soft computing approach on material removal rate in electrochemical discharge machining. Int J Manuf Technol Manag 24:23–39. https://doi.org/10.1504/IJMTM.2011.046758
12. Bindu Madhavi J, Hiremath SS (2016) Investigation on machining of holes and channels on borosilicate and Sodalime glass using μ - ECDM setup. Procedia Technol 25:1257–1264. https://doi.org/10.1016/j.protcy.2016.08.219
13. Yan Z, Zhengyang X, Jun X, Di Z (2016) Effect of tube-electrode inner diameter on electrochemical discharge machining of nickel-based superalloy. Chinese J Aeronaut 29:1103–1110. https://doi.org/10.1016/j.cja.2015.12.016
14. West J, Jhadav A (2007) ECDM methods for fluidic interfacing through thin glass substrates and the formation of spherical microcavities. J Micromech Microeng 17:403–409. https://doi.org/10.1088/0960-1317/17/2/028
15. Jain VK, Adhikary S (2008) On the mechanism of material removal in electrochemical spark machining of quartz. J Mater Process Tech 200:460–470. https://doi.org/10.1016/j.jmatprotec.2007.08.071
16. Peng WY, Liao YS (2004) Study of electrochemical discharge machining technology for slicing non-conductive brittle materials. J Mater Process Tech 149:363–369. https://doi.org/10.1016/j.jmatprotec.2003.11.054
17. Wuthrich R, Fascio V (2005) Machining of non-conducting materials using electrochemical discharge phenomenon — an overview. Int J Mach Tools Manuf 45:1095–1108. https://doi.org/10.1016/j.ijmachtools.2004.11.011
18. Didar TF, Dolatabadi A, Rolf W (2008) Characterization and modeling of 2D-glass micro-machining by spark-assisted chemical engraving ( SACE ) with constant velocity. J Micromech Microeng 18:1–9. https://doi.org/10.1088/0960-1317/18/6/065016
19. Paul L, Hiremath SS (2015) Response surface modeling of micro channels in electrochemical discharge machining process. Appl Mech Mater:238–242. https://doi.org/10.4028/www.scientific.net/AMM.490-491.238
20. Abou JD, Fatanat TD, Rolf W (2012) Micro-texturing channel surfaces on glass with spark assisted chemical engraving. Int J Mach Tools Manuf 57:66–72. https://doi.org/10.1016/j.ijmachtools.2012.01.012
21. Paul L, Hiremath SS (2014) Evaluation of process parameters of ECDM using Grey relational analysis. Procedia Mater Sci 5:2273–2282. https://doi.org/10.1016/j.mspro.2014.07.446
22. Wen KL, Chang TC, You ML (1998) The Grey entropy and its application in weighting analysis. In: SMC'98 conference proceedings. 1998 IEEE International Conference on Systems, Man, and Cybernetics. IEEE Explore, San Diego, CA, USA, 1842–1844. doi: https://doi.org/10.1109/ICSMC.1998.728163
23. Mehrabi F, Farahnakian M, Elhami S, Razfar MR (2018) Application of electrolyte injection to the electro-chemical discharge machining (ECDM) on the optical glass. J Mater Process Tech 255:665–672. https://doi.org/10.1016/j.jmatprotec.2018.01.016
24. Hajian M, Razfar MR, Movahed S, Etefagh AH (2018) Experimental and numerical investigations of machining depth for glass material in electrochemical discharge milling. Precis Eng 51:521–528. https://doi.org/10.1016/j.precisioneng.2017.10.007